Materials Today Communications 29 (2021) 102904

Contents lists available at ScienceDirect

Materials Today Communications

journal homepage: www.elsevier.com/locate/mtcomm

Repeatable mechanical energy absorption of ZnO nanopillars

Jun Wang [a], Min Zhou [b,*], Rong Yang [a], Pan Xiao [a], Fujiu Ke [c], Chunsheng Lu [d]

[a] State Key Laboratory of Nonlinear Mechanics (LNM), Institute of Mechanics, Chinese Academy of Sciences, Beijing 100190, China
[b] G.W.W. School of Mechanical Engineering, Georgia Institute of Technology, Atlanta, GA 30332-0405, United States
[c] School of Physics, Beihang University, Beijing 100191, China
[d] School of Civil and Mechanical Engineering, Curtin University, Perth, WA 6845, Australia

ARTICLE INFO

Keywords:
ZnO nanopillars
Repeatable energy absorption
Phase transformation
Inversion domain boundary
Molecular dynamics

ABSTRACT

We show that repeatable energy absorption can be obtained via the reversible wurtzite-to-hexagonal phase transformation of ZnO nanopillars at room temperature. The effect is demonstrated using molecular dynamics simulations and available experimental data. With uniaxial compressive strains up to 22.1% along the [0001] orientation, a ZnO nanopillar with a lateral dimension of 5.5 nm can produce average specific energy absorption on the order of 26.7 J g^{-1} under quasistatic cyclic loading and 11.1 J g^{-1} under rapid loading. The theoretical maximum of the specific energy absorption is 41.0 J g^{-1} which can be approached at nanopillars with lateral sizes above 55 nm. These values are comparable to that of widely used aluminum foams. The effects of inversion domain boundaries and sample size on the repeatable energy absorbing capacity are discussed. The findings open an avenue for ZnO nanostructures in mechanical energy absorption and dissipation applications.

1. Introduction

The need to remove excessive energy is a prevalent problem in engineering and daily life, e.g., shock absorption in bridges, transport, earthquake resistance of buildings, aircraft landing, running shoes, and noise reduction in precision measurement such as atomic force microscopy and transmission electron microscopy. Such a wide range of demand and application has attracted intensive interest in the development of energy absorbing technologies. The key is designing materials and structures that can dissipate or store mechanical energy. Great efforts have been made in seeking materials and structures with exceptional lightweight [1], deformability [2] and attractive apparent energy absorbing capacity [3,4]. In these studies, the mechanically imposed energy can be either dissipated by heat exchange between a material and the environment during elastic response or stored in materials via plastic deformation. Theoretically, elasticity offers repeatable absorbing opportunities, but the time required to remove the imposed energy is environment dependent. Plastic deformation, however, precludes repeatability as the materials such as metals [5,6] and alloys [7,8] cannot recover their original shapes. Therefore, it is necessary to resort to a different mechanism to achieve reusability.

Reversible phase transformation is such a behavior. It occurs when a material experiences lattice structure changes under external stimulation, often in mechanical or thermal form. The energy absorption and dissipation occur in the transformation process as the interface between the original and new phases moves [9]. Since the material recovers its original size and shape after the transformation reverses, it can be operated for another round of energy absorption. The reversible phase transformations usually occur among polymorphs of a material in which chemical bonds exhibit both covalency and ionicity [10]. It is the non-uniformity of chemical bonds that allows phase transformation to occur through variation of bond angles and change of coordination number of atoms. For bulk materials, cracks may initiate prior to phase transformation due to impurities and defects. For nanomaterials, however, much higher surface-to-volume ratios and the lack of defects in the lattices provide higher atomic mobility, thereby enable phase transformation without failure. Because of this, previously unknown polymorphs and mechanical behaviors have been revealed in a large number of II-VI [11], III-V [12,13] and IV-IV [14] nanomaterials with the pseudoelasticity that can underlie repeatable energy absorption. Among them, ZnO nanostructures have attracted continued interest due to their easy synthesis [15] and application in the field of energy generation [16,17]. In particular, reversible wurtzite-to-hexagonal and wurtzite-to-tetragonal transformations have been predicted by molecular dynamics simulations [18,19] and further confirmed by experiments [20,21] in ZnO nanostructures, in examples that show computations can

* Corresponding author.
E-mail address: min.zhou@gatech.edu (M. Zhou).

https://doi.org/10.1016/j.mtcomm.2021.102904
Received 9 August 2021; Received in revised form 18 October 2021; Accepted 18 October 2021
Available online 22 October 2021

be applied to guide expensive and time-consuming trial-and-error methods in laboratories [22].

In this paper, we combine molecular dynamics simulations with available experimental data to identify a repeatable energy absorbing concept through the reversible wurtzite-to-hexagonal phase transformation of ZnO nanopillars (NPs) subjected to cycles of uniaxial compressive loading and unloading at room temperature. The specific energy absorption obtained by molecular dynamics simulations is verified by experimental data from axial indentation and tension of ZnO nanowires [20,23]. The time expected to revert back to the original wurtzite phase is validated by the hopping frequency between the wurtzite and tetragonal phases previously measured in transmission electron microscope [21]. The absorbing mechanism involves two aspects, dissipation resulting from motion of the interface between the original and new phases as well as storage of configuration energy due to the formation of inversion domain boundaries (IDBs) during the hexagonal-to-wurtzite reverse phase transformation. The former has been well elucidated by previous work [9]. Here, we focus on the latter, as it is the formation of the IDBs and the material size that are responsible for the variation in the average specific energy absorption under different conditions.

2. Model and computational details

The initial ZnO NPs are in the wurtzite phase with a hexagonal cross-sectional shape, six {0110} type lateral crystalline surfaces, and a [0001] axial orientation [24,25]. To ensure traction-free boundary conditions for the lateral surfaces, a vacuum region of 3 nm was maintained outside the lateral surfaces. Periodic boundary conditions were applied along all directions. The lateral dimension of the NPs was chosen to be from 5.5 to 19.8 nm to investigate the effect of size on specific energy absorption per unit weight. The length to lateral dimension ratio was set to 2:1 to avoid buckling.

The partially charged rigid ion model was employed to define the non-Coulombic short-range Zn—O, Zn—Zn and O—O interactions (see Supplementary material) [26]. Thermal properties predicted by the model echo experimental results and therefore the temperature effect on phase transformation can be captured. The model realistically tracks the surface energy, allowing investigation of size-dependent mechanical properties of a NP. The long-range Coulombic interactions were calculated via the Wolf sum [27]. The motion of the atoms was tracked using a Verlet leapfrog algorithm to yield velocities and positions with a time step of 1 fs. The samples were relaxed for 200 ps before compression to arrive at the initial free-standing configurations. To simulate compressive deformation and obtain the mechanical properties of the ZnO NPs, an extra velocity was applied along the [0001] orientation at each integral step via a modified isothermal-isobaric ensemble algorithm [28,29]. This scheme was used to effect a compressive strain rate of 10^9 s^{-1} for the NPs. Strain rates as low as 10^6 s^{-1} were used to explore the strain rate effect on energy absorption of the ZnO NPs. No discernable difference was seen. The stress tensor was calculated by the classical virial formula and the system was maintained at target temperature by the Nosé–Hoover thermostat [30,31]. The configuration energy landscape of various crystalline structures was analyzed using a nudged elastic band method [32]. All simulations were carried out by using a modified version of the DL_POLY package [29].

3. Results

3.1. Wurtzite-to-hexagonal phase transformation

Under ambient conditions, ZnO adopts the wurtzite lattice structure, as illustrated in Fig. 1 which is generated by the VMD software [33]. The wurtzite lattice structure involves tetrahedral bonding with a coordination number of 4 and an O—Zn—O or Zn—O—Zn bonding angle of 109.47°. The wurtzite-to-hexagonal transformation can be obtained from wurtzite ZnO nanostructures via tension along the $[01\bar{1}0]$ or $[2\bar{1}\bar{1}0]$ orientation or compression along the [0001] orientation [18,34]. Under such external stimuli, Zn-cations on the (0001) plane and O-anions on the $(000\bar{1})$ plane tend to move toward each other and bond. As a result, a new Zn—O bond along the $[000\bar{1}]$ orientation forms and 3 of the 4 original tetrahedral Zn—O bonds not in the [0001] direction are compressed flat to within the {0001} plane. Thus, a hexagonal lattice with a coordination number of 5 and two different types of bonding angles are formed. The first type is the 90° bonding angle which consists of 2 Zn—O

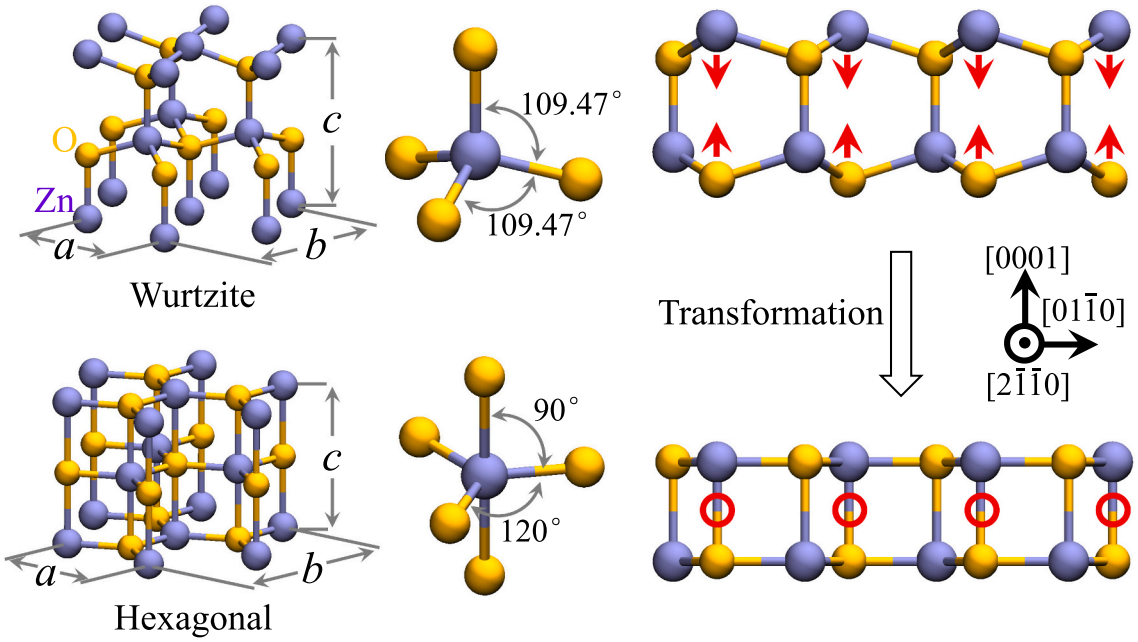

Fig. 1. Wurtzite and hexagonal lattices of ZnO. *a*, *b* and *c* represent lattice constants. Opposite motion (shown by red arrows) of Zn-cations on (0001) plane and O-anions on $(000\bar{1})$ plane causes formation of new bonds (marked by circles) on $(2\bar{1}\bar{1}0)$ plane along $[000\bar{1}]$ orientation, which transforms the original wurtzite structure to a hexagonal one. (For interpretation of the references to color in this figure legend, the reader is referred to the web version of this article.)

bonds along the [0001] and [000$\bar{1}$] orientations, respectively. The second type includes 3 Zn—O bonds mutually forming a 120° bonding angle on the {0001} plane (see Fig. 1).

3.2. Compressive loading and unloading cycle

As shown in Fig. 2, there are three distinct stages in the uniaxial compressive loading curve of a ZnO NP. The first stage (from points A to B) represents elastic compression of the original wurtzite lattice. In the second stage, the wurtzite-to-hexagonal phase transformation is initiated at point B and completed at point C. Fig. 3a shows that nucleation sites are seen throughout the material as the NP is compressed to its elastic limit at a strain of 9.2%. As the strain reaches 9.6%, coalescence of the nucleation sites occurs, leading to regions with the transformed hexagonal structures. The transformed regions grow and merge as the strain increases. As the strain reaches 18.1% (point C in Fig. 2), the entire NP is transformed to the hexagonal lattice structure, except for the surfaces (see Fig. 3a and Supplementary Video S1). Subsequently, the hexagonal-structured NP undergoes elastic compression as strain further increases to 22.1% (from points C to D in Fig. 2). Point D represents the limit of the recoverable strains beyond which failure of the NP would occur. During unloading, the NP first undergoes elastic relaxation from D to E, followed by a hexagonal-to-wurtzite reverse phase transformation (from points E to F in Fig. 2). The last stage of the three-stage unloading process in the stress-strain curve is the elastic recovery in the wurtzite structure from F back to A. However, upon reaching A (zero stress, zero strain), the NP does not fully recover its original single-crystalline wurtzite structure. Instead, the NP is divided into two domains with opposite orientations in the [0001] axial direction by an IDB (see Fig. 3b).

Supplementary material related to this article can be found online at doi:10.1016/j.mtcomm.2021.102904.

The formation of the IDB even after full unloading and recovery can be explained as follows. In the wurtzite-to-hexagonal phase transformation, new Zn—O bonds form along the [000$\bar{1}$] orientation, as shown in Fig. 4. Both the newly formed and the original Zn—O bonds along the [0001] orientation have the same probability to break during the reverse transformation during unloading. Consequently, breaking of the newly formed bonds restores the NP to the initial wurtzite state. However, breaking of an original bond yields the inversion domain (see Fig. 4). The IDB can be eliminated by Zn—O re-bonding along the [000$\bar{1}$] and [0001] orientations with another round of compressive loading. The inset in Fig. 3b shows that an IDB consists of planer four-atom rings with each ring plane perpendicular to the boundary between two oppositely oriented domains. The thickness of the IDB is the Zn—O bond length of 0.2 nm. IDBs are frequently observed in wurtzite II-VI [35,36], III-V [37,38] and IV-IV [39] compounds.

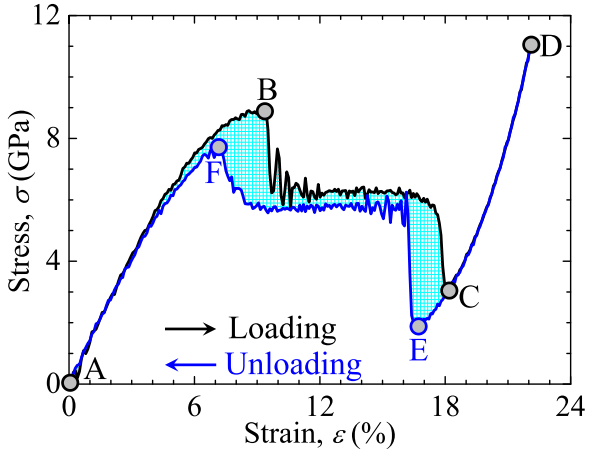

Fig. 2. Uniaxial compressive loading and unloading stress-strain curves of a ZnO NP with a lateral dimension of 5.5 nm at a temperature of 300 K and a loading rate of 10^9 s^{-1}.

Since the unloading path does not overlap with the loading path, as illustrated in Fig. 2, the area of the hysteresis loop is the energy absorbed per unit volume over one cycle of compressive loading and unloading (hereafter referred to as a cycle). The specific energy absorption per unit weight E_a after a cycle can be calculated by

$$E_a = \frac{1}{\rho}\oint \sigma d\varepsilon, \tag{1}$$

where ρ, σ and ε are the mass density of ZnO [40], stress, and strain, respectively. The E_a of the NP with a lateral dimension of 5.5 nm is 29.8 J g^{-1}. It is worth noting here that E_a consists of two parts, dissipation resulting from the motion of the interface between the original and new hexagonal phases [9] and the configuration energy of the IDB.

3.3. Repeatable energy absorption

Fig. 5a shows that E_a fluctuates between 11.1 and 29.9 J g^{-1} as a NP with a lateral dimension of 5.5 nm undergoes 31 cycles of compressive loading and unloading. During the loading part of the second cycle, the IDB resulting from the first cycle is eliminated upon completion of the wurtzite-to-hexagonal phase transformation. This process of IDB generation and elimination causes the fluctuation of E_a in Fig. 5a. Different numbers of IDBs can appear at various places in the NP due to stochastic Zn—O bond-breaking along the [000$\bar{1}$] and [0001] orientations during the unloading part of the cycles, leading the variations in the magnitude of the fluctuation in E_a. Structural analysis indicates that E_a is proportional to the density of IDBs or fraction of atoms structurally involved in IDBs in the NP (see Fig. 5b and c). For example, E_a decreases from 29.8 J g^{-1} in the first cycle to 16.3 J g^{-1} in the second cycle as the IDB concentration decreases from 4.8 at% to 0. In contrast, in the third cycle, E_a increases to 24.9 J g^{-1} as the IDB concentration increases to 4.5 at%. Subsequently, E_a further increases to 26.8 J g^{-1} and the IDB concentration goes up to 7.7 at% in the fourth cycle.

The fluctuation of E_a over the cycles can be understood by the difference in configuration energy landscape between the wurtzite and tetragonal lattices of ZnO. This is because four-atom rings are the building blocks for IDBs. The two Zn—O pairs involved in each four-atom ring has a configuration energy that is 0.11 eV higher than the two Zn—O pairs in a wurtzite lattice (see Supplementary Fig. S1). The IDB concentration change from cycle to cycle allows the change in E_a to be calculated (See Supplementary Eq. (S8)). For example, from the third to fourth cycle, the change in E_a is 2.1 J g^{-1} (Supplementary Eq. (S8)). This is very close to the result of 26.8–24.9 = 1.9 J g^{-1} from the simulation.

The two parts comprising E_a can also be evaluated using Supplementary Eq. (S8). For instance, after the first cycle, the IDB concentration change is 4.8%. The contribution of this change to E_a is thus calculated to be 3.1 J g^{-1}, which accounts for 10.4% of E_a. Therefore, the energy dissipated by the motion of the interface between the original wurtzite and resulting hexagonal phase is 29.8–3.1 = 26.7 J g^{-1} (89.6% of E_a). This implies that E_a can be maintained at least at this value overall many cycles even if IDBs are fully removed after each cycle. This assumes interfaces between the original wurtzite and new hexagonal structures behavior the same way throughout the cycles. This is the long cycle expected value for E_a. Note that Fig. 5b shows that the IDB concentration can indeed be zero at times, such as in the second, 10th and 22nd cycles. After such points, E_a invariably goes up.

3.4. Thermal stability of an IDB

Annealing is a classic technique to eliminate undesirable structures in a system [41]. To estimate the time required to remove an IDB, the NP

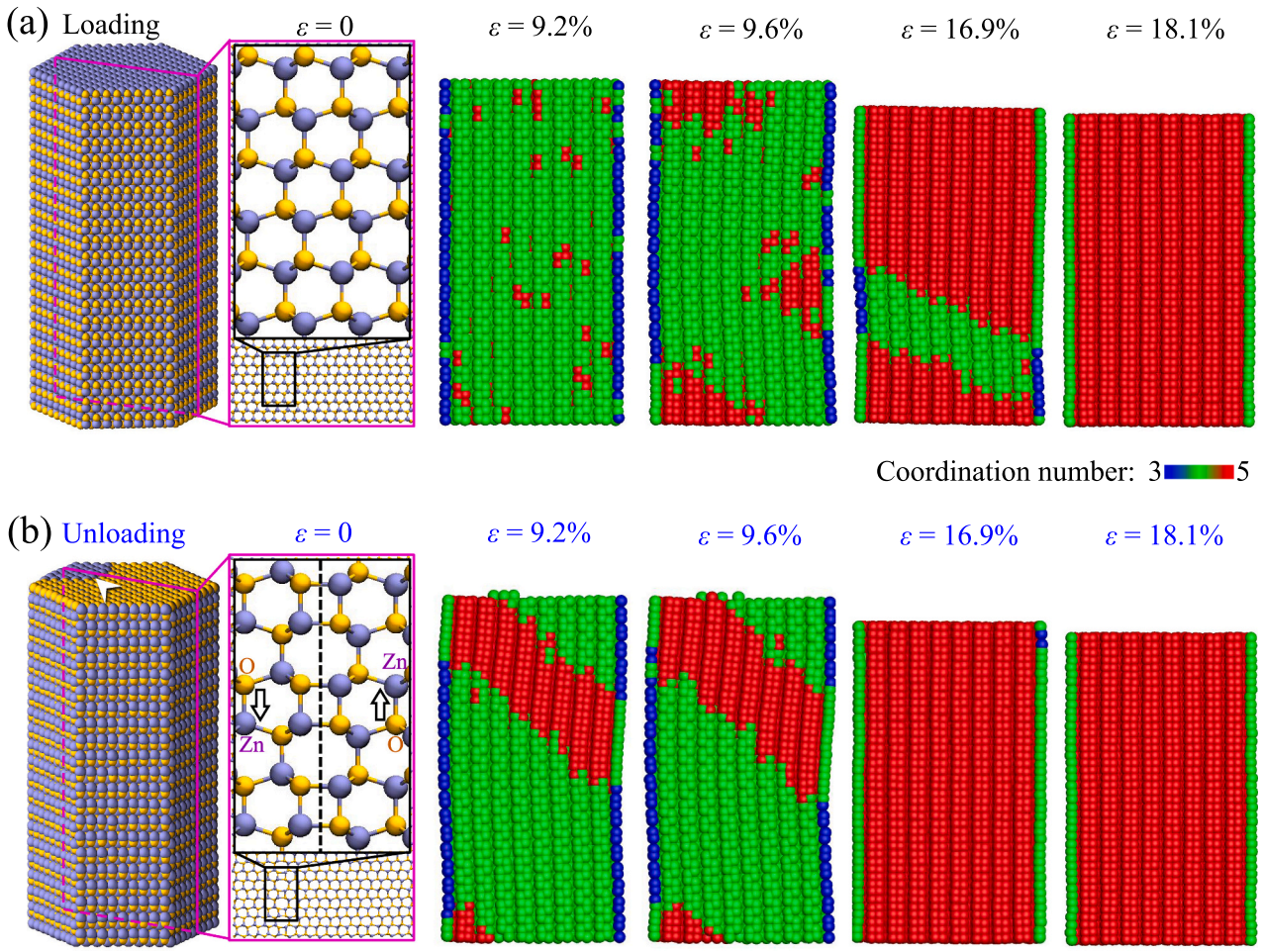

Fig. 3. Cross-sectional patterns of a NP under (a) loading and (b) unloading at various strains. Coordination numbers of 3, 4 and 5 correspond to atoms belonging to surface, wurtzite and hexagonal lattices, respectively. Insets show partially enlarged structures of the original wurtzite and an IDB (denoted by a dashed line). The inversion domain is marked by an arrowhead. Hollow arrows show opposite orientations of Zn—O bonds at two sides of the IDB.

was annealed after the first cycle at temperatures in the range of 600–900 K. The structure evolution at 600 K is shown in Fig. 6a, where a 4-step hop leads to the annihilation of the IDB at the surface of the NP. Each step corresponds to 1/2 lattice unit along the $[01\bar{1}0]$ orientation, with a displacement of $\sqrt{3}a/2$ (a is the lattice constant of wurtzite ZnO, see Supplementary Fig. S2a and Video S2). The time required is 660 ns. For a travel distance of d, the time t expected to observe annihilation at temperature T is

$$t = \frac{d}{\sqrt{3}a/2}\frac{1}{\gamma_0}e^{\frac{\Delta Q}{k_B T}}, \tag{2}$$

where ΔQ is the activation energy of an IDB, k_B and γ_0 are the Boltzmann constant and vibrational frequency of ZnO, respectively. For $\Delta Q = 0.76$ eV (Supplementary Fig. S2b) and $\gamma_0 = 10^{13}$ s^{-1}, which are upper limit values for optical phonons of wurtzite ZnO [42,43], Eq. (2) gives predictions that track simulation results at various temperatures (see Fig. 6b).

Supplementary material related to this article can be found online at doi:10.1016/j.mtcomm.2021.102904.

Since an energy absorbing device is most likely operated at room temperature, it is more practical to extrapolate the time expected to eliminate an IDB at 300 K. Based on our simulations, Eq. (2) predicts that the time is 2.3 s (see Fig. 6b). This value is on the same order of magnitude as the time scale (~ 10 s) of a reversible wurtzite-to-tetragonal phase transformation experimentally observed in ZnO nano-islands at room temperature [21]. Note also that the density functional theory calculation has put the energy barrier between wurtzite and tetragonal ZnO at 0.96 eV [21]. This value yields a time of 1340 s for a transformation event from a four-atom ring to two wurtzite Zn—O pairs at 300 K, much longer than the simulation prediction and experimental observation at room temperature. The density functional theory is independent from experiments and molecular dynamics. However, the interatomic interactions used in the latter are determined by fitting to mechanical and physical properties that are experimentally measured or partially predicted by the density functional theory [26]. Therefore, the time to annihilate an IDB derived from the density functional theory deviates from the molecular dynamics and experimental data.

3.5. Size effect

An analysis of the behavior of ZnO NPs with a range of lateral dimensions is carried out. The result shows that E_a increases monotonically from 29.8 to 39.2 J g^{-1} as the lateral dimension D increases from 5.5 to 19.8 nm (see Fig. 7). This is due to the reduction in the ratio between surface atoms and volume atoms as D increases. As shown in Fig. 3, the surface region with a thickness of one atomic layer does not participate in the phase transformation and thus has no contribution to energy absorption. If the thickness of the surface region remains the same at a, E_a can be written as a function of size D as

$$E_a = E_a^0\left(1 - \frac{a}{D/2}\right)^2, \tag{3}$$

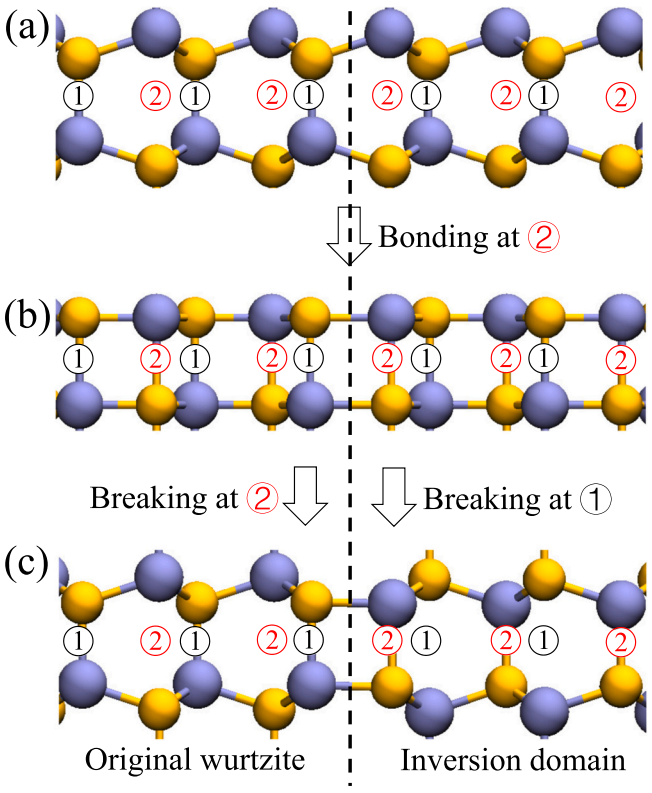

Fig. 4. Formation of an IDB. (a) Original wurtzite and (b) transformed hexagonal structures and (c) two domains with opposite orientations divided by an IDB. Symbols ① and ② denote sites of the original and new formed Zn—O bonds. The dashed line marks position of the IDB. Bonding at ② transforms the original wurtzite structure to a hexagonal one. Bond-breaking at ② restores the original wurtzite region. However, bond-breaking at ① produces an inversion domain.

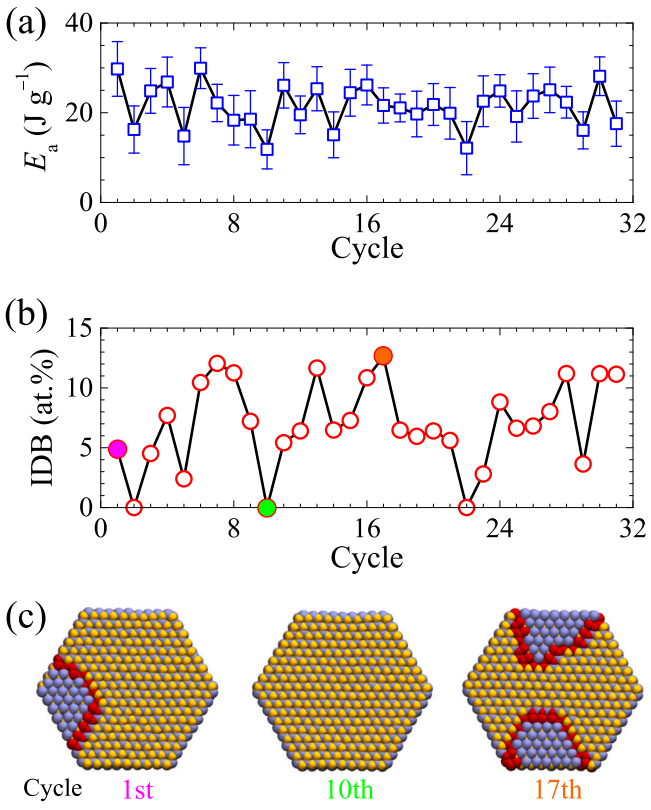

Fig. 5. (a) The specific energy absorption per unit weight and (b) atomic percentage of IDBs during 31 cycles of compressive loading and unloading. (c) Lateral patterns with IDBs outlined in red after the first, 10th and 17th cycles.

where $E_a^0 = 41.0$ J g^{-1} is the theoretical maximum of E_a as D approaches infinity, or the specific energy absorption of bulk wurtzite-structured ZnO if the forward and reverse phase transformations could happen. Eq. (3) is very consistent with our simulation results (see Fig. 7). It is important to point out that the E_a for a nanowire estimated from available experimental data (Supplementary Eq. (S16)) also coincides with Eq. (3) at $D = 55$ nm.

4. Discussion

The hysteresis loop in the stress-strain relation in Fig. 2 associated with the reversible wurtzite-to-hexagonal phase transformation is typical of pseudoelastic material behavior due to a range of underlying mechanisms. The reversible phase transformation consumes energy to overcome the energy barrier between the original wurtzite and new hexagonal phases, leading to the hysteresis loop. Such relations have also been seen in the axial indentation force-displacement relations of ZnO nanowires in atomic force microscopy experiments [20]. Such relations allow the energy absorption to be assessed. The nanowires in Ref. [20] have length to lateral dimension ratios around 10:1, therefore, undergo buckling during axial indentation. This is an inefficient configuration for energy absorption, as only the compressive side of the bent wires can undergo the wurtzite-to-hexagonal transformation. In addition, the tensile side can experience brittle fracture. Experiments show that the tensile fracture stain of wurtzite-structured ZnO nanowires is in the range of 2–15% [23,44–46]. This gives rise to a high degree of uncertainty in the extent of wurtzite-to-tetragonal phase transformation that can happen in ZnO nanowires under indentation. The critical buckling strain of a nanowire also deviates from the prediction of the classical Euler buckling theory due to the lateral size effect [47]. Because of these reasons and to avoid buckling, we believe the optimal aspect ratio for energy absorption should be as low as it could be, e.g., 2:1 for the slender NP analyzed here.

The part of the energy dissipated through the propagation of the interface between the original wurtzite and transformed hexagonal phases has been well elucidated previously [9]. The part that is associated with the formation of IDBs in the form of configuration energy fluctuates as the occurrence of the IDBs does not fully coincide with the loading-unloading cycles. Although for a particular cycle, IDBs can enhance or reduce the specific energy absorption depending on the starting and ending structure details, overall the occurrence of IDBs lowers the energy dissipation capacity of the ZnO NPs. Since IDBs are thermally unstable, they can spontaneously annihilate at the surfaces of a NP with the expected time scale depending on the lateral size of the NPs and temperature. The thermal energy in the form of lattice vibrations measured by the temperature enables the transformation to overcome the energy barrier between the wurtzite and tetragonal phases, facilitating the motion of an IDB. Therefore, higher temperatures correspond to faster annihilation of an IDB. Analysis shows that, at room temperature, the time is on the order of 2.3 s for an IDB which is 1.1 nm from the surface of a NP. This estimate is on the same order as the tetragonal-to-wurtzite transformation time of ~ 10 s experimentally measured in ZnO nano-islands at room temperature [21]. Taken together, the simulations and the experiments suggest that the E_a of NPs with a lateral dimension of ~ 5.5 nm can be maintained at a relative stable value for load-unload cycles with periods longer than ~ 2.3 s (~ 0.4 Hz) to allow sufficient inter-cycle structural relaxation or recovery. Under such conditions, E_a can be on the order of 26.7 J g^{-1}, representing the long cycle expected value. If the NPs with a lateral dimension of 5.5 nm are operated at frequencies higher than ~ 0.4 Hz, E_a is at least 11.1 J g^{-1} which is the high-frequency lower limit.

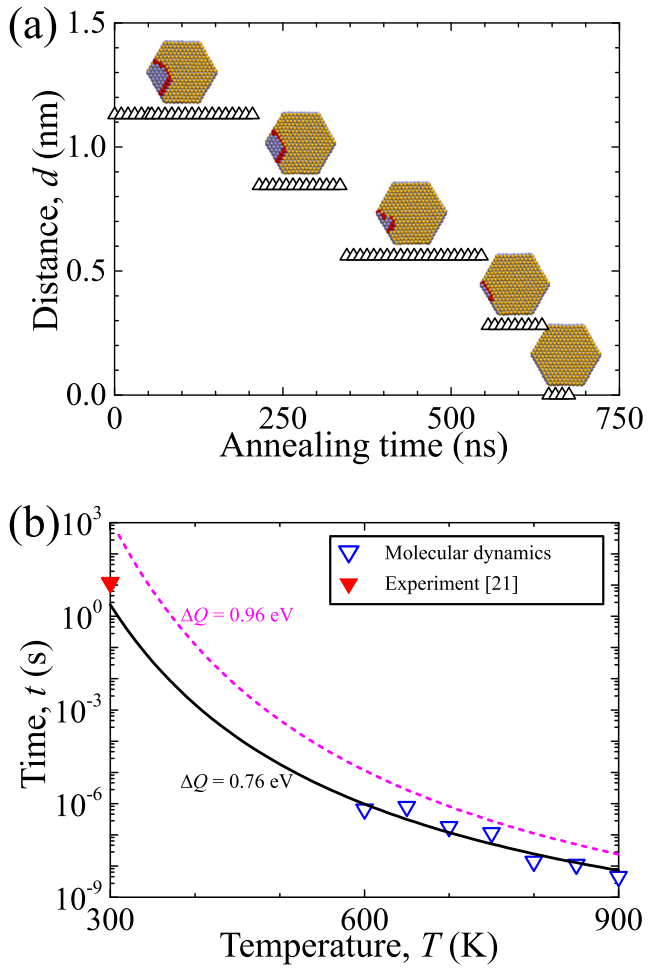

Fig. 6. Thermal stability of an IDB. (a) The distance from an IDB to surface of a NP reduces with annealing time at 600 K. Insets show lateral patterns with an IDB marked in red. (b) Time to remove an IDB versus temperature. The solid and dash curves are theoretical predictions of Eq. (3) with 0.76 eV (the activation energy of the IDB obtained by the present study) and 0.96 eV (the energy barrier between the four-atom ring and two Zn—O pairs of the wurtzite cell from the density functional theory [21]). (For interpretation of the references to color in this figure legend, the reader is referred to the web version of this article.)

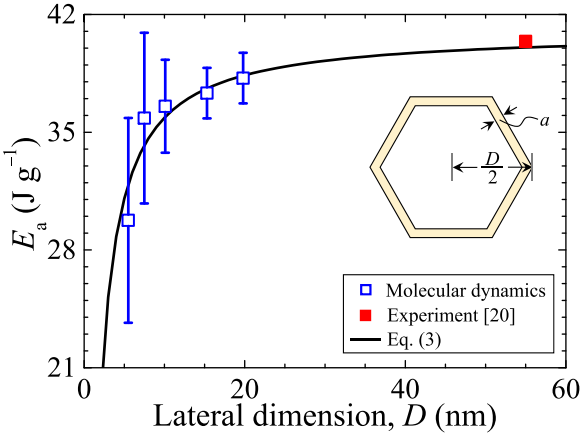

Fig. 7. Size effect on energy absorption of ZnO nanopillars. An inset sketches a core-shell model in which the outer shell of a nanopillar does not contribute to energy absorption.

So far, two types of IDBs have been experimentally observed in wurtzite-structured ZnO. One type is along the {0001} planes due to dopants such as Sn and Sb [35] and the other type occurs on the {0110} planes in pristine ZnO [36]. Our analysis involves the latter.

The theoretical maximum of E_a is 41.0 J g^{-1} which can be seen in NPs with large lateral dimensions. The experimental data in Ref. [20] suggests that NPs with a lateral dimension of 55 nm have an E_a of 40.8 J g^{-1} (Supplementary Eq. (S16)). This provides a practical guide for the choice of lateral dimension as it suggests that lateral sizes of more than 55 nm offer no further significant enhancement in E_a. It is also worth noting that the values of E_a of ZnO NPs are comparable to those of conventional energy absorbing materials such as aluminum and alloy syntactic foams [48,49]. Recently, well aligned ZnO nanowire arrays have been synthesized with tunable inter-wire distances [24,25], thus demonstrating that the overall material density of ZnO NP arrays can be tailored as the building blocks of energy absorbing devices (see Fig. 8). Since reversible phase transformation has been identified in a large number of II-VI [11], III-V [12,13] and IV-IV [14] nanomaterials, their potential exploitation with similar effects as that in ZnO NPs can be identified and studied in the future.

5. Conclusion

We have shown that [0001]-orientated ZnO NPs possess an ability to repeatedly absorb mechanical energy during cycles of uniaxial compressive loading and unloading. This ability is due to the reversible phase transformation between wurtzite and hexagonal lattice structures at the nanoscale. The analysis uses molecular dynamics simulations and available experimental data. The specific energy absorption of NPs over the size range of 5.5–55 nm is quantified from the hysteretic stress-strain and force-displacement relations, in particular with the 5.5 nm case associated with the cyclic loading and unloading.

The energy absorbing mechanisms include dissipation through motion of the interface between the original wurtzite and new hexagonal phases and the storage of configuration energy in IDBs. Energy absorption fluctuates through cycles due to changes in the concentration of IDBs. The analyses here have established the theoretical maximum which can be approached at NPs with lateral sizes above 55 nm, long cycle expected value, and high-frequency lower limit of the specific energy absorption. IDBs can spontaneously move and annihilate over time scales of several seconds at room temperature. These findings provide guidance for designing mechanical energy absorbing devices using ZnO NPs.

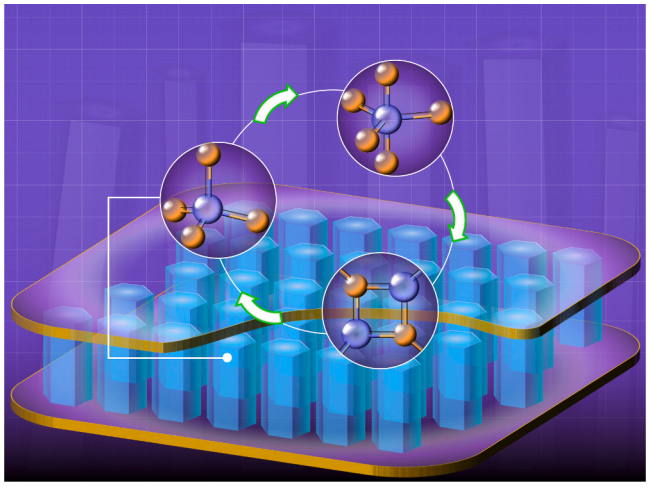

Fig. 8. A concept of a repeatable energy absorbing device based on a ZnO nanopillar array.

CRediT authorship contribution statement

Jun Wang: Conceptualization, Investigation, Methodology, Data curation, Writing – original draft, Writing – review & editing, Funding acquisition. **Min Zhou:** Supervision, Guidance, Writing – review & editing, Revision, Finalization. **Rong Yang:** Formal analysis, Writing – review & editing. **Pan Xiao:** Funding acquisition, Writing – review & editing. **Fujiu Ke:** Methodology. **Chunsheng Lu:** Formal analysis, Validation, Writing – review & editing.

Declaration of Competing Interest

The authors declare that they have no known competing financial interests or personal relationships that could have appeared to influence the work reported in this paper.

Acknowledgments

This work was supported by the National Natural Science Foundation of China (Grant Nos. 11772332 and 11790292), the Strategic Priority Research Program of the Chinese Academy of Sciences (Project No. XDB22040501) and the Opening Fund of State Key Laboratory of Nonlinear Mechanics. Computations were performed on resources provided by the Pawsey Supercomputing Center with funding from the Australian Government and the Government of Western Australia, the LNMGrid of the State Key Laboratory of Nonlinear Mechanics, and the ScGrid of Supercomputing Center, Computer Network Information Center of the Chinese Academy of Sciences.

Appendix A. Supplementary material

Supplementary data associated with this article can be found in the online version at doi:10.1016/j.mtcomm.2021.102904.

References

[1] J.B. Berger, H.N.G. Wadley, R.M. McMeeking, Mechanical metamaterials at the theoretical limit of isotropic elastic stiffness, Nature 543 (2017) 533–537.
[2] L.R. Meza1, S. Das, J.R. Greer, Strong, lightweight, and recoverable three-dimensional ceramic nanolattices, Science 345 (6202) (2014) 1322–1326.
[3] L.J. Yi, T.C. Chang, X.Q. Feng, Y.Y. Zhang, J. Wang, B. Hua, Giant energy absorption capacity of graphene-based carbon honeycombs, Carbon 118 (2017) 348–357.
[4] C. Tang, Q. Zhang, M.Q. Zhao, G.L. Tian, F. Wei, Resilient aligned carbon nanotube/graphene sandwiches for robust mechanical energy storage, Nano Energy 7 (2014) 161–169.
[5] F. Shuang, K.E. Aifantis, Using molecular dynamics to determine mechanical grain boundary energies and capture their dependence on residual Burgers vector, segregation and grain size, Acta Mater. 195 (2020) 358–370.
[6] F. Shuang, K.E. Aifantis, Modelling dislocation-graphene interactions in a BCC Fe matrix by molecular dynamics simulations and gradient plasticity theory, Appl. Surf. Sci. 535 (2021), 147602.
[7] X.W. Li, T. Shi, B. Li, X.C. Chen, C.W. Zhang, Z.G. Guo, Q.X. Zhang, Subtractive manufacturing of stable hierarchical micro-nano structures on AA5052 sheet with enhanced water repellence and durable corrosion resistance, Mater. Des. 183 (2019), 108152.
[8] X.W. Li, J.S. Liang, T. Shi, D.N. Yang, X.C. Chen, C.W. Zhang, Z.H. Liu, D.Z. Liu, Q. X. Zhang, Tribological behaviors of vacuum hot-pressed ceramic composites with enhanced cyclic oxidation and corrosion resistance, Ceram. Int. 46 (9) (2020) 12911–12920.
[9] A.J. Kulkarni, M. Zhou, Continuum characterization of novel pseudoelasticity of ZnO nanowires, J. Mech. Phys. Solids 56 (7) (2008) 2473–2493.
[10] J.C. Phillips, Ionicity of the chemical bond in crystals, Rev. Mod. Phys. 42 (3) (1970) 317–356.
[11] B. Fu, L. Chen, Y. Xie, J. Feng, X. Ye, Novel mechanical behaviors of wurtzite CdSe nanowires, J. Nanopart. Res. 17 (2015), 354-67.
[12] B. Wen, J. Zhao, R. Melnik, Y. Tian, Body-centered tetragonal B2N2: a novel sp3 bonding boron nitride polymorph, Phys. Chem. Chem. Phys. 13 (32) (2011) 14565–14570.
[13] K. Jung, M. Cho, M. Zhou, Structure and thermomechanical behavior of bent GaN nanowires, Comput. Mater. Sci. 81 (2014) 524–529.
[14] Y. Fujimoto, T. Koretsune, S. Saito, T. Miyake, A. Oshiyama, A new crystalline phase of four-fold coordinated silicon and germanium, New J. Phys. 10 (2008), 083001.
[15] Z.W. Pan, Z.R. Dai, Z.L. Wang, Nanobelts of semiconducting oxides, Science 291 (5510) (2001) 1947–1949.
[16] Z.L. Wang, J.H. Song, Piezoelectric nanogenerators based on zinc oxide nanowire arrays, Science 14 (5771) (2006) 242–246.
[17] P.C. Lee, Y.L. Hsiao, J. Dutta, R.C. Wang, S.W. Tseng, C.P. Liu, Development of porous ZnO thin films for enhancing piezoelectric nanogenerators and force sensors, Nano Energy 82 (2021), 105702.
[18] A.J. Kulkarni, M. Zhou, K. Sarasamak, S. Limpijumnong, Novel phase transformation in ZnO nanowires under tensile loading, Phys. Rev. Lett. 97 (10) (2006), 105502.
[19] J. Wang, A.J. Kulkarni, K. Sarasamak, S. Limpijumnong, F.J. Ke, M. Zhou, Molecular dynamics and density functional studies of a body-centered-tetragonal polymorph of ZnO, Phys. Rev. B 76 (17) (2007), 172103.
[20] M. Ghosh, S. Ghosh, H. Attariani, K. Momeni, M. Seibt, G.M. Rao, Atomic defects influenced mechanics of II−VI nanocrystals, Nano Lett. 16 (10) (2016) 5969–5974.
[21] M.R. He, R. Yu, J. Zhu, Reversible wurtzite–tetragonal reconstruction in ZnO (100) surfaces, Angew. Chem. Int. Ed. 51 (31) (2012) 7744–7747.
[22] M. Zhou, Exceptional properties by design, Science 339 (6124) (2013) 1161–1162.
[23] R. Agrawal, B. Peng, E.E. Gdoutos, H.D. Espinosa, Elasticity size effects in ZnO nanowires-a combined experimental-computational approach, Nano Lett. 8 (11) (2008) 3668–3674.
[24] C.C. Zhao, A.Q. Chen, X. Ji, Y. Zhu, X.C. Gui, F. Huang, Z.K. Tang, Growth of vertically aligned ZnO nanowire arrays on ZnO single crystals, Mater. Lett. 154 (2015) 40–43.
[25] R. Hollinger, D. Gupta, M. Zapf, R. Röder, D. Kartashov, C. Ronning, C. Spielmann, Single nanowire defined emission properties of ZnO nanowire arrays, J. Phys. D Appl. Phys. 52 (29) (2019), 295101.
[26] S.W. Wang, Z.C. Fan, R.S. Koster, C.M. Fang, M.A. van Huis, A.O. Yalcin, F. D. Tichelaar, H.W. Zandbergen, T.J.H. Vlugt, New ab initio based pair potential for accurate simulation of phase transitions in ZnO, J. Phys. Chem. C 118 (20) (2014) 11050–11061.
[27] D. Wolf, P. Keblinski, S.R. Phillpot, J. Eggebrecht, Exact method for the simulation of Coulombic systems by spherically truncated, pairwise r^{-1} summation, J. Chem. Phys. 110 (17) (1999) 8254–8282.
[28] S. Melchionna, G. Ciccotti, B.L. Holian, Hoover NPT dynamics for systems varying in shape and size, Mol. Phys. 78 (3) (1993) 533–544.
[29] W. Smith, C.W. Yong, P.M. Rodger, DL_POLY: applications to molecular simulation, Mol. Simul. 28 (5) (2002) 385–471.
[30] S. Nosé, A molecular dynamics method for simulations in the canonical ensemble, Mol. Phys. 52 (2) (1984) 255–268.
[31] W.G. Hoover, Canonical dynamics: equilibrium phasespace distribution, Phys. Rev. A 31 (3) (1985) 1695–1697.
[32] G. Henkelman, H. Jónsson, Improved tangent estimate in the nudged elastic band method for finding minimum energy paths and saddle points, J. Chem. Phys. 113 (22) (2000) 9978–9985.
[33] W. Humphrey, A. Dalke, K. Schulten, VMD: visual molecular dynamics, J. Mol. Graph. 14 (1) (1996) 33–38.
[34] P.L. Zhao, X.X. Guan, H. Zheng, S.F. Jia, L. Li, H.H. Liu, L.L. Zhao, H.P. Sheng, W. W. Meng, Y.L. Zhuang, J.B. Wu, L.Y. Li, J.B. Wang, Surface-and strain-mediated reversible phase transformation in quantum-confined ZnO nanowires, Phys. Rev. Lett. 123 (21) (2019), 216101.
[35] V. Ribić, A. Rečnik, M. Komelj, A. Kokalj, Z. Branković, M. Zlatović, G. Branković, New inversion boundary structure in Sb-doped ZnO predicted by DFT calculations and confirmed by experimental HRTEM, Acta Mater. 199 (2020) 633–648.
[36] Y.Z. Liu, H.T. Yuan, Z.Q. Zeng, X.L. Du, X.D. Han, Q.K. Xue, Z. Zhang, Inversion domain boundary in a ZnO film, Philos. Mag. Lett. 87 (9) (2007) 687–693.
[37] P. Xiao, X. Wang, J. Wang, F.J. Ke, M. Zhou, Y.L. Bai, Surface transformation and inversion domain boundaries in gallium nitride nanorods, Appl. Phys. Lett. 95 (21) (2009), 211907.
[38] N. Li, S. Labat, S.J. Leake, M. Dupraz, J. Carnis, T.W. Cornelius, G. Beutier, M. Verdier, V. Favre-Nicolin, T.U. Schulli, O. Thomas, J. Eymery, M.I. Richard, Mapping inversion domain boundaries along single GaN wires with Bragg coherent x-ray imaging, ACS Nano 14 (8) (2020) 10305–10312.
[39] W.R.L. Lambrecht, B. Segall, Electronic-structure study of the (110) inversion domain boundary in SiC, Phys. Rev. B 41 (5) (1990) 2948–2958.
[40] S.C. Abrahams, J.L. Bernstein, Remeasurement of the structure of hexagonal ZnO, Acta Crystallogr. B25 (1969) 1233–1236.
[41] S. Hong, C.S. Lee, M.H. Lee, Y. Lee, K.Y. Ma, G. Kim, S.I. Yoon, K. Ihm, K.J. Kim, T. J. Shin, S.W. Kim, E. Jeon, H. Jeon, J.Y. Kim, H.I. Lee, Z. Lee, A. Antidormi, S. Roche, M. Chhowalla, H.J. Shin, H.S. Shin, Ultralow-dielectric-constant amorphous boron nitride, Nature 582 (2020) 511–514.
[42] J. Wang, Y.G. Shen, F. Song, F.J. Ke, X.Z. Liao, C. Lu, On the wurtzite to tetragonal phase transformation in ZnO nanowires, Nanotechnology 28 (16) (2017), 165705.
[43] Z. Wang, F. Wang, L. Wang, Y. Jia, Q. Sun, Firstprinciples study of negative thermal expansion in zinc oxide, J. Appl. Phys. 114 (6) (2013), 063508.
[44] M.R. He, P. Xiao, J. Zhao, S. Dai, F.J. Ke, J. Zhu, Quantifying the defect-dominated size effect of fracture strain in single crystalline ZnO nanowires, J. Appl. Phys. 109 (2011), 123504.
[45] R. Agrawal, B. Peng, H.D. Espinosa, Experimental-computational investigation of ZnO nanowires strength and fracture, Nano Lett. 9 (12) (2009) 4177–4183.
[46] S. Hoffmann, F. Östlund, J. Michler, H.J. Fan, M. Zacharias, S.H. Christiansen, C. Ballif, Fracture strength and Young's modulus of ZnO nanowires, Nanotechnology 18 (20) (2007), 205503.

[47] J. Wang, Y.G. Shen, F. Song, F.J. Ke, Y.L. Bai, C. Lu, Size-dependent brittle-to-ductile transition in GaAs nano-rods, Eng. Fract. Mech. 150 (2015) 135–142.
[48] G.Y. Sun, S.F. Li, Q. Liu, G.Y. Li, Q. Li, Experimental study on crashworthiness of empty/aluminum foam/honeycomb-filled CFRP tubes, Compos. Struct. 152 (2016) 969–993.
[49] J. Meng, T.W. Liu, H.Y. Wang, L.H. Dai, Ultra-high energy absorption high-entropy alloy syntactic foam, Compos. Part B Eng. 207 (2021), 108563.